Journal of Animal & Plant Sciences, 35(4): 2025, Page: 900-915
ISSN (print): 1018-7081; ISSN (online): 2309-8694
https://doi.org/10.36899/JAPS.2025.4.0078

EFFECTS OF BONE MARROW-DERIVED MESENCHYMAL STEM CELLS-LOADED SELF-ASSEMBLING PEPTIDE SCAFFOLD ON SYNOVIAL VOLUME AND CARTILAGE THICKNESS ON RABBIT MODEL OF RHEUMATOID ARTHRITIS

R.N. Sha[1] and J. Z. Li[2*]

[1]Department of Medicine, Ordos Institute of Technology, Ordos, 017000, Inner Mongolia Autonomous Region, China;
[2]Medical Imaging Center, Qingdao University Affiliated Taian City Central Hospital, Taian, 271000, Shandong, China.
*Corresponding author's email: ljizheng@yeah.net

ABSTRACT

This study was to assess the potential therapeutic effects of bone marrow-derived mesenchymal stem cells (BMSCs) loaded onto self-assembling peptide scaffolds on the rabbit model of rheumatoid arthritis (RA). The morphology of prepared BMSCs self-assembling peptide scaffold with the capability for loading was observed and cell biocompatibility was assessed. A total of sixty New Zealand white rabbits were utilized to establish RA model and were randomly rolled into Control group, Bracket group, BMSCs group and Negative group. In Control group, the joint was exposed surgically (joint exposure procedure) but was not subjected to any therapeutic intervention, while in Bracket group, the peptide scaffold was placed into the joint. In BMSCs group, BMSCs-loaded peptide scaffolds were implanted into the joints. The Negative group received no treatment, undergoing neither surgical procedures nor any therapeutic intervention, maintaining the normal physiological state. The extent of joint swelling was measured and assessed in rabbits. MRI scans of the rabbit knee joints were performed to evaluate the status of the synovium and cartilage. Hematoxylin-Eosin (HE) was performed on rabbit joint cartilage tissues to assess the post-treatment cartilage tissue status. ELISA was utilized for measurement of inflammatory factor levels in the rabbits. Western blotting was conducted to assess key protein expressions. The peptide hydrogel showed excellent biocompatibility. MRI evaluation showed that the volume of synovial hyperplasia in BMSCs group was significantly lower than that in Control group and Bracket group ($P \leq 0.05$), and cartilage thickness increased significantly over time, reaching 0.91 ± 0.07 mm at 3 months ($P \leq 0.05$). ELISA analysis indicated that the levels of inflammatory cytokines (tumor necrosis factor(TNF)-α, interleukin(IL)-1β, IL-6, C-reactive protein(CRP)) in BMSCs group were significantly lower than those in Control group and Bracket group ($P \leq 0.05$). Western blotting results demonstrated that the expression of COL2A1 protein was increased in BMSCs group (0.89 ± 0.09 *vs. c*ontrol group 0.44 ± 0.07, $P \leq 0.05$), while the expression of cartilage oligomeric matrix protein(COMP) was significantly decreased (0.89 ± 0.11 *vs c*ontrol group 0.64 ± 0.08, $P \leq 0.05$). HE staining revealed that after 3 months of BMSCs treatment, cartilage thickness increased, chondrocyte proliferation was significant, matrix staining was well-preserved, and no vascularity was observed. Both synovial pathology scores and Mankin scores for cartilage indicated that the pathological damage in BMSCs group was significantly improved ($P \leqslant 0.05$), with better outcomes compared to Bracket group. BMSCs-loaded self-assembling peptide scaffold has potential therapeutic effects on rabbit model of RA, especially in terms of reducing synovial overgrowth and promoting cartilage repair.

Keywords: rheumatoid arthritis; bone marrow-derived mesenchymal stem cells; self-assembling peptide scaffolds;MRI; rabbit model

Published first online June 10, 2025 Published final July 29, 2025

INTRODUCTION

Rheumatoid arthritis (RA) is characterized primarily by arthritis and systemic symptoms (Radu and Bungau, 2021; Nagy *et al*., 2021; Yang *et al*., 2022). The main symptoms of this disease include joint pain, swelling, stiffness, and functional impairment (Hansildaar *et al*., 2021; Kerschbaumer *et al*., 2020). The treatment goals for RA are pain relief, inflammation alleviation, improvement in function, and prevention of joint damage (Deane and Holers, 2021). Traditional approaches to RA therapy include non-steroidal anti-inflammatory drugs, glucocorticoids, immunomodulatory agents, and physical therapy and joint replacement surgery. Nevertheless, these treatments provide symptomatic relief, are not curative, and come with certain side effects and risks.

The New Zealand White rabbit is one of the ideal experimental animals for constructing RA models, offering advantages such as a high success rate in model

establishment, ease of evaluating modeling outcomes, and suitability for various research purposes, including new drug development, disease mechanism exploration, and drug treatment efficacy assessment. To improve the treatment outcomes of RA, researchers have begun exploring the use of scaffolds for repairing damaged synovium and cartilage. Commonly utilized scaffold materials include autologous bone marrow-derived mesenchymal stem cells (BMSCs) and peptide scaffolds (Yamanaka, 2020; Parmar *et al*., 2020). These scaffolds exhibit excellent biocompatibility and biological activity, promoting the regeneration and repair of synovium and cartilage. Among them, BMSCs self-assembling peptide scaffold represents a novel therapeutic approach (Chia *et al*., 2020; Chen *et al*., 2020; Pan *et al*., 2022). It combines BMSCs with peptide scaffolds, forming a three-dimensional structure that provides better support and an environment conducive to cell growth and differentiation. BMSCs possess pluripotency and self-renewal capabilities, capable of differentiating into various cell types, including chondrocytes and synovial cells (Liang *et al*., 2023). Peptide scaffolds offer a suitable microenvironment that enhances the growth and differentiation of BMSCs and exhibit excellent biocompatibility and biological activity (Hou *et al*., 2022). Nevertheless, there are still some issues regarding the application of BMSCs self-assembling peptide scaffolds in the treatment of RA (Xie *et al*., 2021; Jiao *et al*., 2021). Firstly, the fabrication methodologies for these scaffolds remain unclear and require further research and improvement. Secondly, more experiments and clinical studies are needed to validate the effectiveness and safety of scaffold usage in RA treatment.

This study aimed to assess the effects of BMSCs-loaded self-assembling peptide scaffolds on synovial membrane volume and cartilage thickness on rabbit model of RA, so as to explore their potential in RA treatment.

MATERIALS AND METHODS

Fabrication of BMSCs peptide scaffolds: Ten milligrams of RADA16-I peptide (Peptide Institute, Inc., Japan) were dissolved in a 10% sterile sucrose solution to prepare a 1% peptide solution (by water bath, until fully dissolved). BMSCs cell suspension was applied to the solution and incubated at 37°C for 30 minutes to promote self-assembly into a stable peptide scaffold structure. Subsequently, 250 μL of DMEM/F12 medium(Sigma-Aldrich, USA)was supplemented, and gentle pipetting with a 200 μL pipette tip was performed to ensure thorough mixing of the peptide solution and the culture medium, resulting in a final concentration of 0.5%. The microtubes were placed in a 37°C incubator for 30 minutes to observe the self-assembly of the peptide. To further visualize the self-assembly of the peptide, a small amount of the peptide mixture solution was placed on a cover glass, and 0.1 mol/L $CaCl_2$ solution was applied to visualize the self-assembly of the peptide.During the preparation of the peptide scaffolds, no crosslinking agents were used. The RADA16-I peptide formed a stable self-assembled structure through intermolecular interactions.

Observation of peptide scaffold structure and biocompatibility testing: The dissolved peptide solution was dispersed and impurities were removed using an ultrasonic cleaner (40 KHz, 25°C, 10 minutes). It was then diluted to a concentration of 0.01% (w/v). Subsequently, 5 μL of the 0.01% (w/v) peptide solution was gently dropped onto the center of a mica sheet for 25-30 seconds, followed by gentle rinsing with 50 μL of PBS buffer 2-3 times, and air-dried. The samples were examined using an PointProbe Atomic Force Microscope (NanoWorld, Switzerland) with the following parameters: acceleration voltage 0.5-30 kV, scan frequency 70 kHz, scan speed 1.0-1.2 Hz, spring constant 2.8 N/m, lateral resolution 0.1 nm, and tip curvature radius 10-225 μm. Topomatrix image analysis software was utilized to measure and analyze the scan results.

Biocompatibility testing was performed using the CCK-8 assay on the BMSCs cell suspension prepared in section 2.5.2, and logarithmically growing cells were utilized for the experiment. The cell suspension, prepared with DMEM-F12, was seeded into a 96-well plate. The culture plate was pre-incubated in a cell culture incubator for 24 hours (37°C, 5% CO_2). According to the instructions of the CCK-8 Cell Proliferation and Toxicity Detection Kit (Sigma-Aldrich, USA), the supernatant was discarded, and 10μL of CCK-8 solution was applied, followed by incubation for 2 hours (37°C, 5% CO_2). The absorbance at 450 nm was measured employing a microplate reader (the measurements were taken on day 1, 3, 5, and 7, with one plate taken out for measurement on each day).

Animals and grouping: Sixty New Zealand white rabbits (male, 8 weeks old, with body weight ranging from 1.5 to 1.8 kg; DiLi Animal Science and Technology Co., Ltd., Heze, Shandong, China) were selected for this study. Prior to modeling, all the rabbits were housed under standard conditions (temperature at 20±2°C, relative humidity at 55±5%, 12 hours of light per day with low intensity, good ventilation, and noise levels below 60 decibels). They were fasted for 12 hours and deprived of water for 6 hours before modeling. All experiments were approved by Ethics Committee of Ordos Institute of Technology (Inner Mongolia Autonomous Region, China), and in accordance with the Guide for the Care and Use of Laboratory Animals published by the United States National Institutes of Health.

The rabbits were randomly divided into four groups (with 15 rabbits in each group): Control group (the joints were surgically exposed but received no therapeutic intervention), Bracket group (peptide scaffolds placed within the joint), BMSCs group (peptide scaffolds loaded with BMSCs implanted into the joint), and Negative group (remained untreated, undergoing neither surgical procedures nor therapeutic interventions, maintaining the normal physiological state). After grouping, each group of rabbits underwent experimental procedures according to the corresponding treatment protocol.

Preparation of RA model: A RA model was induced using ovalbumin (Sigma-Aldrich, USA). Ovalbumin was dissolved in physiological saline (Gibco, USA) to prepare a solution with a concentration of 20 g/L. It was then mixed with an equal volume of Freund's adjuvant (Sigma-Aldrich, USA)and injected subcutaneously on the back of rabbits once a week for three consecutive weeks to sensitize them. One week after the last injection, 5 mg of ovalbumin dissolved in physiological saline was injected into the right hind knee joint of the rabbits. After injection, the rabbits were placed in standard animal housing cages for free movement and feeding, and observed for any abnormalities other than those at the research site. Modeling success was confirmed if acute inflammatory signs such as redness, swelling, heat, and pain occurred in the injected joint within 24 hours.

Following successful modeling, the experiments were conducted. Control group underwent exposure treatment at the surgical site only. Bracket group had the peptide scaffold inserted into the joint, while BMSCs group had peptide scaffolds containing BMSCs inserted into the joint.

Extraction and preparation of BMSCs: The rabbits were anesthetized by intravenous injection of 2 mL/kg isoflurane (Abbott Laboratories Limited, USA)via the auricular vein. After the surgical area was shaved, the tibia of the rabbits was exposed under sterile conditions, and a sterile needle was utilized to puncture the bone marrow cavity, aspirating bone marrow fluid into a sterile centrifuge tube. Subsequently, the bone marrow fluid was mixed with DMEM/F12 in proportion to dilute it. Low-speed centrifugation (2 min, 1,000 rpm) was then performed to separate the mononuclear cell layer, followed by two washes (5 min, 1,000 rpm) with serum-free cell culture medium. The separated bone marrow mesenchymal cells were transferred to DMEM/F12 medium to form a single-cell suspension of BMSCs.

MRI evaluation: After the placement of the scaffold in the surgery, MAGNETOM Skyra 3.0TMagnetic Resonance Imaging System (SIEMENS, Germany) of the rabbit's hind knee joint were conducted at the 1st, 2nd, and 3rd months. The rabbits were securely positioned on the operating table, and intraperitoneal injection of 25 mg/kg pentobarbital sodium (Sigma-Aldrich, USA) was administered to ensure they were in an unconscious and painless state. The rabbits were placed in a left lateral decubitus position with the right knee elevated and secured using sandbags. Volumetric imaging was performed in the sagittal plane using a circularly polarized flexible surface coil. Three-dimensional fat-suppressed fast imaging with steady-state precession (3D-FS-FISP) and three-dimensional fat-suppressed spoiled gradient echo (3D-FS-SPGR) sequences were utilized for the plain scanning phase, with the addition of a fat-suppressed 3D-FLASH sequence for contrast-enhanced scanning. Changes in synovial membrane volume and cartilage thickness of the right posterior knee joint were observed. The area of the thickened synovium in each original image was measured layer by layer to calculate the volume. Continuous measurements of the thickness of the right posterior knee cartilage were taken, and the average thickness was calculated.

Swelling of joints: A flexible tape measure was utilized to measure the joint circumference at the modeling site before modeling and on the 6th, 12th, 18th, and 24th days post-modeling to assess the degree of swelling. On the 24th day, an infrared thermometer was utilized to measure skin temperature at a point 2 cm from the midpoint of the line connecting the inner and outer condyles of the rabbit's femur. The thermal hyperalgesia threshold was measured by stimulating the rabbit's knee joint with PL-200Hot Stinger Pain Instrument (Chengdu Taimeng Software Co., Ltd., China). The time from the start of stimulation to the rabbit's struggle or avoidance was recorded as the pain threshold, and this measurement was taken three times and averaged.

Analysis of inflammatory factor levels: ELISA was employed to measure tumor necrosis factor-alpha (TNF-α), interleukin (IL)-1β, IL-6, and C-reactive protein (CRP) in rabbit samples. Each sample was measured in triplicate, and the average value was used as the final result. Prior to modeling, five randomly selected rabbits were assigned as Control group (normal). All test kits were purchased from Shanghai COIBO Biotechnology Co., Ltd., China. On the 24th day post-modeling, five rabbits each from Control group, Bracket group, and BMSCs group were randomly chosen and anesthetized with intraperitoneal injection of 2 mL/kg isoflurane. Following anesthesia, 5 mL of blood was collected from the abdominal aorta and the serum was separated by centrifugation. The experimental procedures were carried out according to the instructions provided with the assay kit, and the absorbance was measured at 450 nm employing an ELISA reader to calculate the content.

Western blotting: After the rabbits were anesthetized, the right knee surgical area was cleaned. A 1.5 cm

incision was made approximately 1.5 cm above and below the right rabbit's knee joint, and a whole section of the femoral condyle, tibial plateau, and joint capsule tissues was extracted. The joint tissues were placed in a cryogenic tissue homogenizer, added with 100 μL of ice-cold RIPA buffer (Beijing Solarbio Technology Co., Ltd., China), and then centrifuged and sonicated for cell disruption. The mixture was heat-treated in a water bath (100°C, 7 min). Protein concentration was determined using BCA assay (Shandong Qizhuo New Materials Technology Co., Ltd., China). A 10% SDS-PAGE gel solution was prepared, and the protein samples from the supernatant were mixed with β-mercaptoethanol and sample buffer. Electrophoresis was conducted after heating (95°C, 5 min). Blotting was performed using 5% skim milk. Anti-Collagen II Ab and Anti-Cartilage Oligomeric Matrix Protein Ab were applied separately, diluted at 1:5,000 and 1:1,000, respectively (Sigma-Aldrich, USA). After 12 hours, the primary Abs were removed, and Anti-Rabbit IgG (H+L) HRP Conjugate was applied as the secondary Ab(Sigma-Aldrich, USA), diluted at 1:500, and incubated for 2 hours. Washes were performed three times for 5 minutes each using PBS with Tween 20 (PBST). Visualization was carried out using an ECL chemiluminescent substrate (Thermo Barnstead, USA), and the images were captured using the APX100 digital imaging system. *Image J* was utilized to measure the optical density of individual protein bands, which were then versus the intensity of β-actin.

Observation of staining of articular cartilage tissue: For each group, 5 non-repeating rabbits were selected at 1 and 3 months post-treatment for further observation of joint tissues using Hematoxylin-Eosin (HE) staining. The process of extracting joint tissues was the same as described in Section 2.6. After joint extraction, rabbits were allowed to recover from anesthesia, their vital signs were monitored, appropriate care was provided, and their health was continuously assessed. Rabbit joint tissues were rinsed with pre-cooled PBS buffer. The cartilage tissue was fixed in 4% paraformaldehyde (OriGen, USA). The cartilage tissue was gradually dehydrated in a series of graded ethanol solutions to remove water content. After dehydration, the tissue was embedded in paraffin and sliced into thin sections of 5 μm thickness using a microtome. Deparaffinization and HE staining were performed, followed by dehydration and clearing in ethanol solutions. Pathological morphological evaluations were conducted using optical microscope (Nikon Biomicroscope NI, Japan).

Synovial pathology score: The proliferation of the synovial lining layer, the degree of inflammation in the lower lining layer, and the extent of vascularization are critical indicators for assessing disease severity and progression. Scoring for these parameters was performed at 1, 2, and 3 months post-treatment. The cumulative total of these three scores represents the pathological total score, utilized to assess the severity and progression of synovial diseases. The evaluation criteria are as follows: (1) Proliferation of the synovial lining layer is scored based on cell number, with ≤3 cells receiving 0 points, 3-4 cells receiving 1 point, 5-6 cells receiving 2 points, and >6 cells receiving 3 points (Arora and Robey, 2022). (2) Synovial inflammation is assessed by the presence and distribution of inflammatory cells, with a score of 0 for no inflammatory cells, 1 point for few inflammatory cells, 2 points for diffuse distribution, and 3 points for the formation of lymphatic follicles or germinal centers (Liu *et al*., 2021; Kelly *et al*., 2020). (3) Synovial blood vessels are evaluated based on neovascularization, with a score of 0 for no neovascularization, 1 point for mild neovascularization, 2 points for moderate neovascularization, and 3 points for severe neovascularization (Reda *et al*., 2021).

Cartilage Mankin score: The Mankin scoring system (Tian *et al*., 2019) for cartilage is a commonly utilized methodology for assessing the extent of cartilage tissue damage. Scoring was performed at 1, 2, and 3 months post-treatment. The Mankin scoring system evaluates cartilage damage across four aspects: cartilage structure, cell status, cell distribution, and matrix staining. Scores range from 0 to 14 points, with higher scores indicating more severe cartilage degeneration. Based on the scores, cartilage can be categorized as follows: 0 point: normal cartilage; 1-2 points: mild cartilage damage; 3-6 points: moderate cartilage damage; 7-10 points: severe cartilage damage; 11-14 points: profound cartilage damage. To minimize the influence of subjective factors on the scoring results, a blind method was implemented for the researchers responsible for the Mankin scoring. The researchers were unaware of the group allocation of the samples during the evaluation process. The samples were numbered and randomly assigned to the observers for scoring. After all the samples were scored, the data were subsequently compiled and analyzed, ensuring that the researchers were blinded to the group information during the scoring process.

Statistical Analysis: Statistical analysis was conducted using SPSS 26.0 to process and analyze quantitative data. Quantitative data were presented as mean ± standard deviation, with the mean represented as x and the standard deviation as s. For comparing means among multiple groups, a one-way analysis of variance followed by the least significant difference test was employed. When comparing means between two independent groups, a two-sample t-test was applied. Statistical significance was determined at a significance level of $P \leq 0.05$.

RESULTS

Peptide scaffold structure and biocompatibility test results: According to the test results, the dissolved peptide exhibited a colorless and transparent gel-like appearance (Fig. 1A). Microstructural observations of the peptide revealed the presence of numerous nanofibers within it (Fig. 1B). Fig. 1C shows the morphology of BMSCs cells prepared before the CCK-8 assay. Under microscopic observation, the cells exhibited irregular textures and shapes. Fig. 1D presents the proliferation curves of BMSCs cells from four groups as measured by the CCK-8 assay. The data indicated that, over time, the A value of BMSCs group increased most significantly, with differences observed at multiple time points compared to the other groups ($P \leq 0.05$). This suggests that the peptide scaffold significantly enhanced cellular metabolic activity ($P \leq 0.05$). CCK-8 results demonstrated that the peptide scaffold significantly enhanced cellular metabolic activity ($P \leq 0.05$), making it a safe and reliable scaffold material.

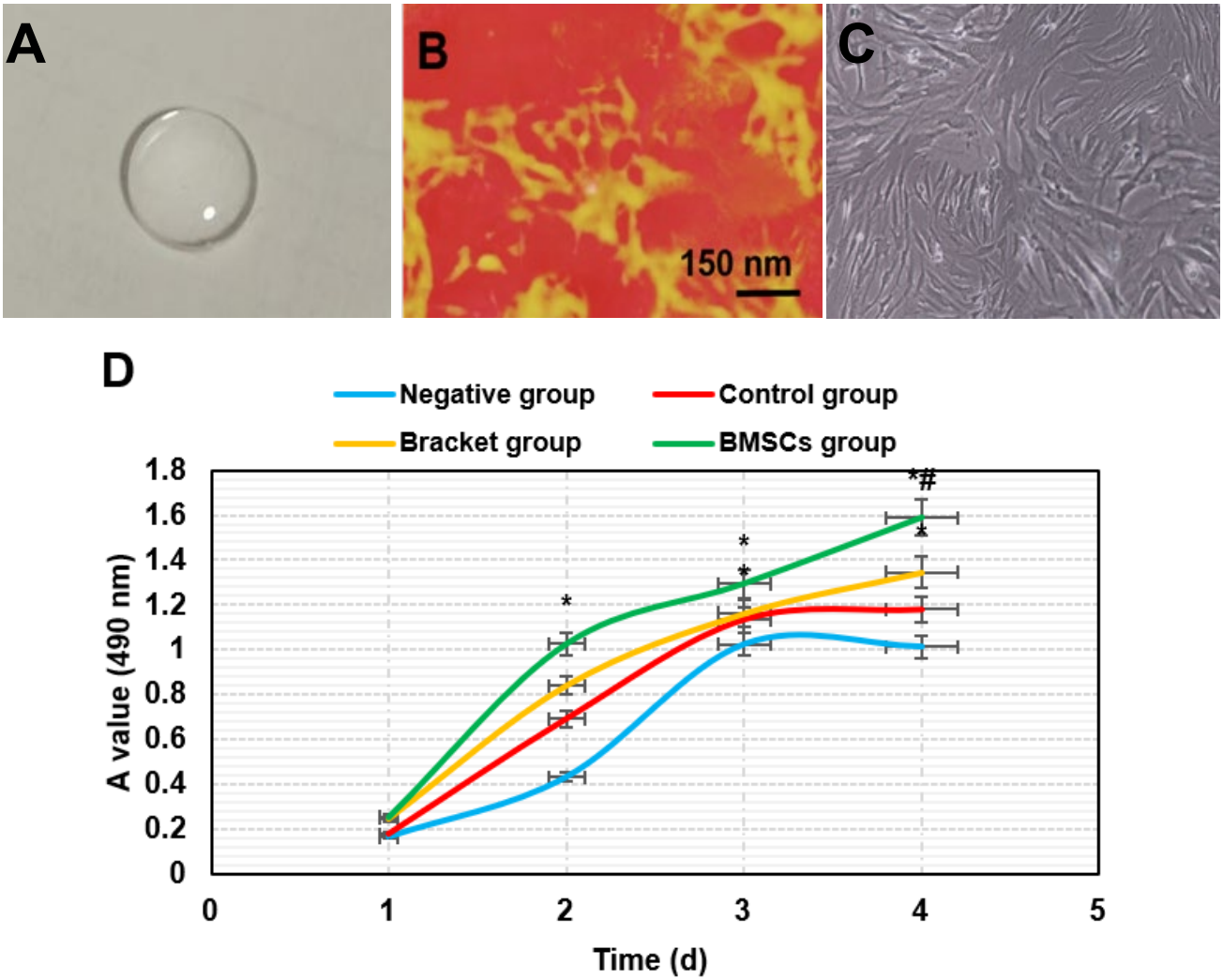

Fig 1. Physicochemical properties and biocompatibility of peptide scaffolds. A: peptide scaffold containing 0.1 mol/L $CaCl_2$; B: atomic force microscopy images of 0.01% peptide solution; C: BMSCs cell morphology prepared before CCK-8 experiment; D: CCK-8 detected the proliferation curves of BMSCs cells in four groups. *$P \leq 0.05$ vs. Control group; #$P \leq 0.05$ vs. Bracket group.

General condition of rabbits: The Negative group exhibited no joint swelling. The degree of joint swelling in rabbits post-modeling is illustrated in Fig. 2A. At day 6 post-modeling, the joint circumference reached its maximum value in all fourgroups and gradually decreased over time. Nevertheless, Bracketgroup and BMSCs group exhibited a drastic reduction in joint swelling versus Control group ($P \leq 0.05$), with BMSCs

group also displaying a greatly inferior degree of swelling to Bracket group ($P \leq 0.05$). By day 24 post-modeling, the joint skin temperature and pain threshold of the rabbits were both correlated with the degree of joint swelling. In Fig. 2B, the pain threshold of Negative group was the lowest, while the pain threshold of BMSCs group was the highest. Furthermore, both Bracketgroup and BMSCs groups showed significant differences compared to Negative groupand Control group ($P \leq 0.05$), indicating that Bracket and BMSCs may play a role in increasing the pain threshold. In Fig. 2C, the skin temperature of Negative group was the lowest, while the skin temperature of BMSCs group was the highest. Moreover, both Bracket groupand BMSCs group exhibited significant differences in skin temperature compared to Negative groupand Control group ($P \leq 0.05$), suggesting that Bracket and BMSCs may influence skin temperature. Greater joint circumference corresponded to more severe joint swelling, along with lower skin temperature, and notably inferior pain thresholds to rabbits with mild joint swelling ($P \leq 0.05$).

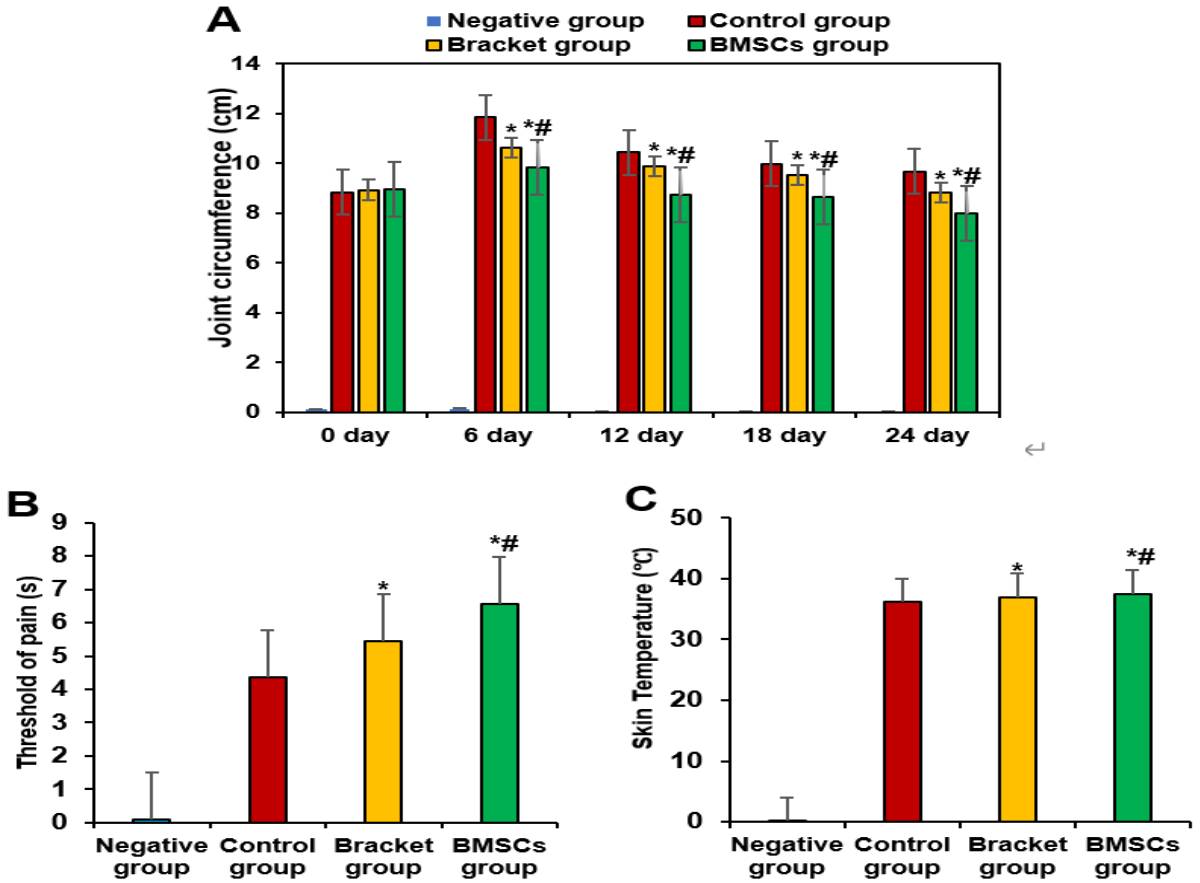

Fig 2. General condition of rabbits. A: degree of joint swelling; B: relationship between the degree of joint swelling and pain threshold; C: relationship between the degree of joint swelling and skin temperature.*$P \leq 0.05$ vs. Control group; #$P \leq 0.05$ vs. Bracketgroup.

Magnetic resonance observation results:MRI examinations of the hind limb knee joints of rabbits were conducted at 1, 2, and 3 months post-treatment using a superconducting magnetic resonance scanner (Fig. 3). Normal synovium did not exhibit any abnormalities in any of the MRI sequences. In the 3D-FS-FISP and FS-3D-FLASH sequences, the articular cartilage appeared as high-signal, arc-shaped structures, surrounding the cortical bone of the femoral condyles and tibial plateaus. These high-signal areas displayed uniform signal distribution with smooth and well-defined edges. During the first month after establishment of the RA model, there were minimal differences in MRI images among the fourgroups, all of which exhibited synovial thickening. Nevertheless, after three months of treatment, while all fourgroups demonstrated an overall increase in synovial thickness, the synovium in Control group exhibited notable thickening. In contrast, the synovial thickening in BMSCs group was substantially inferior to that in Bracket group and Control group ($P \leq 0.05$) (Fig. 3A). The volume of synovial thickening significantly increased in Control group, whereas it was greatly lower in Bracket

group versus Control group. Moreover, BMSCs group displayed markedly lower synovial thickening volume versus both Control group and Bracket group ($P \leq 0.05$).

In Fig. 3B, at 1, 2, and 3 months, the effusion thickness in BMSCs group was significantly lower than that in Controlgroup and Bracket group ($P \leq 0.05$). Specifically, at 1 month, the effusion thickness was (1.3 ± 0.1) mm in Control group, (0.9 ± 0.1) mm in Bracket group, and (0.4 ± 0.2) mm in BMSCs group; at 2 months, it was (1.11 ± 0.1) mm inControl group, (0.8 ± 0.3) mm in Bracket group, and (0.3 ± 0.2) mm in BMSCs group; at 3 months, it was (1.0 ± 0.2) mm in Control group, (0.6 ± 0.2) mm in Bracket group, and (0.4 ± 0.2) mm in BMSCs group.

In Fig. 4A, at 1 month of treatment, the cartilage thickness in Negative group was (0.32 ± 0.04) mm, in Control group was (0.52 ± 0.03) mm, in Bracket group was (0.56 ± 0.04) mm, and in BMSCs group was (0.62 ± 0.05) mm. At 2 months of treatment, the cartilage thickness in Negative group was (0.29 ± 0.04) mm, in Control group was (0.47 ± 0.04) mm, in Bracket group was (0.60 ± 0.03) mm, and in BMSCs group was (0.81 ± 0.06) mm. At 3 months of treatment, the cartilage thickness in Negative group was (0.29 ± 0.04) mm, in Control group was (0.39 ± 0.05) mm, in Bracket group was (0.65 ± 0.04) mm, and in BMSCs group was (0.91 ± 0.07) mm. The differences between BMSCs group and both Controlgroup and Bracket group were statistically significant ($P \leq 0.05$).

In Fig. 4B, MRI scans of the hind limb knee joints of the rabbits were performed at 1, 2, and 3 months. Fig. 4B(a-d) shows Negative group, Control group, Bracket group, and BMSCs group, respectively. The red arrows indicated the locations where cartilage thickness was measured, and 3D-FS-FISP sequences were used for scanning. From the images, it was clearly visible that BMSCs group exhibited a significant increase in cartilage thickness. The normal control group (Negative group) did not show any abnormalities in the synovium or cartilage in any of the MRI sequences. In the 3D-FS-FISP and FS-3D-FLASH sequences, the joint cartilage appeared as a high-signal arc-shaped structure surrounding the cortical bone of the femoral condyle and tibial plateau, with uniform signal distribution and smooth, clear edges. During the experiment, there were no significant changes in synovial or cartilage thickness in Negative group. Compared to Negative group, Control group showed thickening of the synovium and thinning of the cartilage after modeling; the Bracket group and BMSCs group showed reduced synovial thickening and increased cartilage thickness after treatment, with BMSCs group showing more significant changes ($P \leq 0.05$). During the establishment of the experimental model, all fourgroups of rabbits exhibited cartilage thinning. Nevertheless, after three months of treatment, the cartilage in Control group rabbits continued to thin, while the group with the scaffold exhibited a gradual increase in joint cartilage thickness. In contrast, the group with loaded BMSCs with self-assembling peptide scaffolds demonstrated a substantial restoration of joint cartilage thickness, approaching normal levels. The evolution of cartilage changes in rabbits during the experiment is depicted in Fig. 4, illustrating a significant increase in cartilage thickness in the RA model treated with loaded BMSCs with self-assembling peptide scaffolds. This suggests that loaded BMSCs with self-assembling peptide scaffolds have the capacity to promote cartilage repair and regeneration. BMSCs possess multipotent differentiation potential, allowing them to differentiate into chondrocytes and generate cartilage matrix.

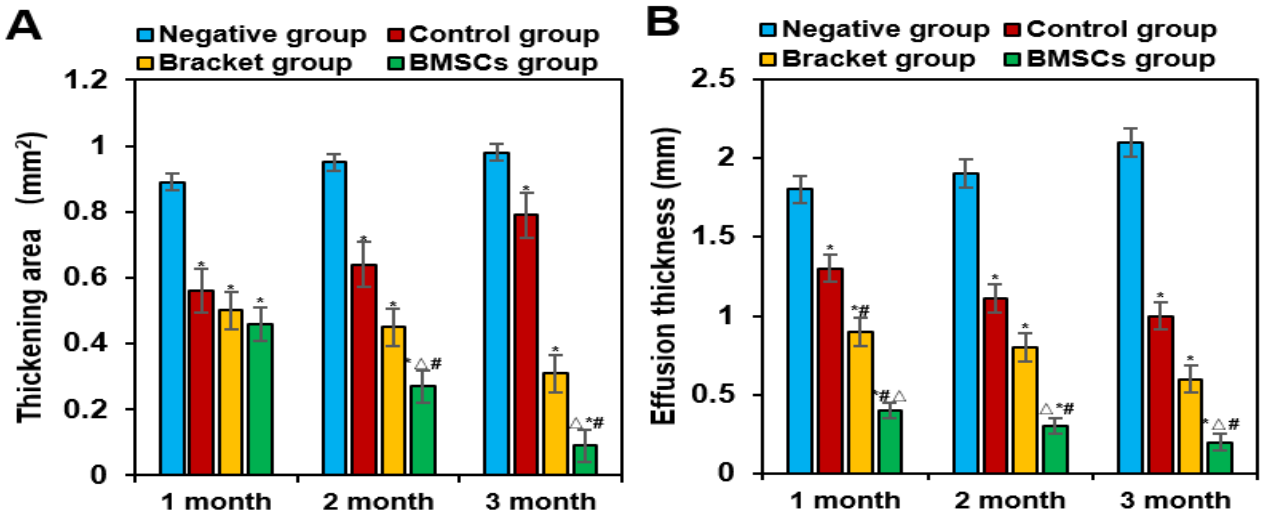

Fig 3. Comparison of MRI images and synovial thickening volume in each group.

A: thickening area, B: effusion thickness; *$P \leq 0.05$ vs. Negative group; #$P \leq 0.05$ vs. Control group; Δ$P \leq 0.05$ vs. Bracket group.

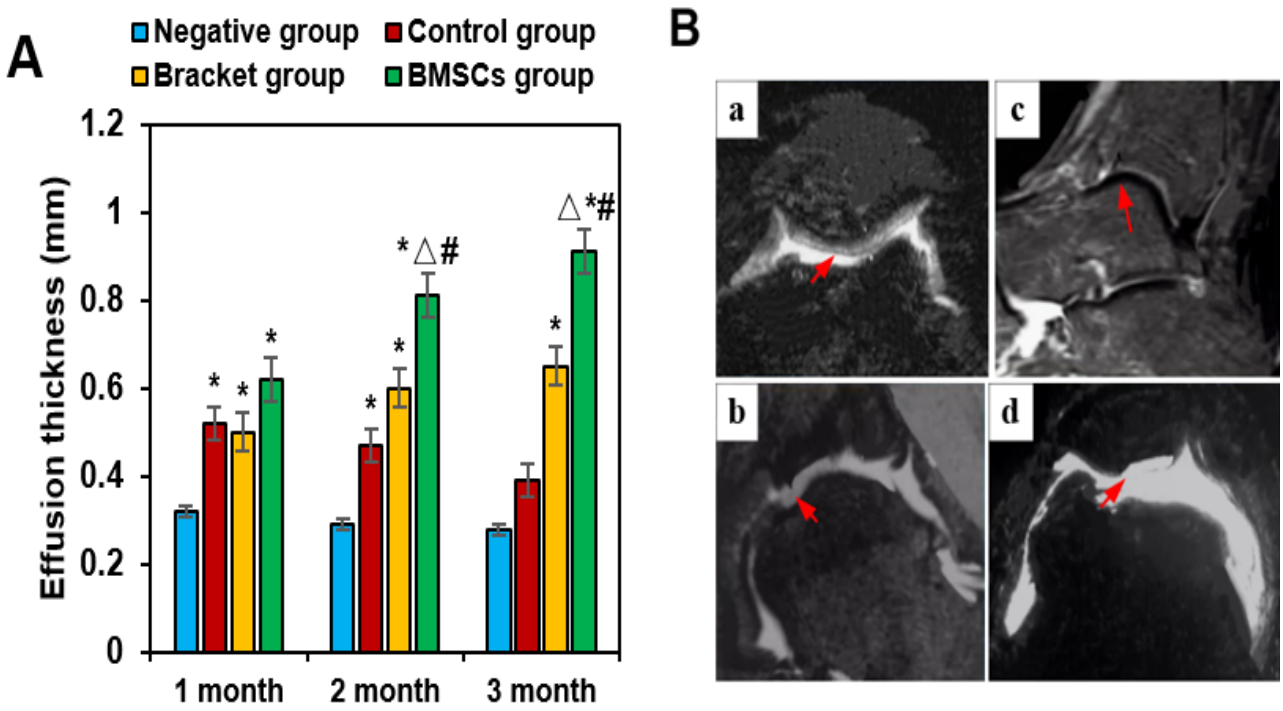

Fig 4. Comparison of changes in articular cartilage thickness in each group of rabbits. A: cartilage thickness; B:MRI images. a:Negative group; b:Controlgroup; c: Bracket group; d: BMSCs group.**P*≤0.05 vs. Negative group; #*P*≤0.05 vs.Control group; Δ*P*≤0.05 vs. Bracket group.

Analysis of inflammatory factor levels: The results are shown in Fig. 5, where the levels of inflammatory markers were significantly reduced in BMSCs group. In Negative group, the TNF-α level was (471.43 ± 50.21) pg/mL, IL-1β was (32.105 ± 5.12) pg/mL, IL-6 was (45.000 ± 6.23) pg/mL, and CRP was (13.500 ± 2.15) mg/L. After modeling, the levels of these inflammatory markers were significantly increased in Control group (*P*≤0.05). However, in BMSCs groupand Bracket group, the levels of inflammatory markers were significantly lower than those in Control group after treatment (*P*≤0.05). In Negative group, the levels of TNF-α, IL-1β, IL-6, and CRP were markedly superior to those in Control group (*P*≤0.05) (Fig. 5). In contrast, both Bracketgroup and BMSCs group exhibited considerably inferior levels to Control group (*P*≤0.05), with BMSCs group also showing remarkably inferior levels to Bracket group (*P*≤0.05).

Western blotting results: In Fig. 6A, the cartilage oligomeric matrix protein(COMP)content in Negative group was (0.99 ± 0.01), in Control group was (0.64 ± 0.08), in Bracket group was (0.73 ± 0.10), and in BMSCs group was (0.89 ± 0.11) (Fig. 6A). The differences between Controlgroup and Bracket group compared to Negative group were significant (*P*≤0.05). The COMP content in the joints of Control group was significantly higher than in Bracket group and BMSCs group (P≤0.05), and the differences between BMSCs group and both Controlgroup and Bracket group were also significant (*P*≤0.05).

In Fig. 6B, the COL2A1 protein content in Negative group was (0.99 ± 0.02), in Control group was (0.44 ± 0.07), in Bracket group was (0.78 ± 0.10), and in BMSCs group was (0.89± 0.09). The differences between Control group and Bracket group compared to Negative group were significant (*P*≤0.05). The COL2A1 protein content in the joints of Control group was significantly higher than in Bracket group and BMSCs group (*P*≤0.05), and the differences between BMSCs group and both Controlgroupand Bracket group were also significant (*P*≤0.05). Fig. 6C shows the Western Blot results, which were used to detect the expression of specific proteins in different groups. β-actin served as the internal reference gene. Based on the intensity of the bands, it can be observed that the expression of COMP and COL2A1 was relatively higher in Negative groupand BMSCs group, while the expression in Control groupand Bracket group was comparatively weaker. COL2A1 is a key component of articular cartilage, and an increase in its content indicates enhanced synthesis of the cartilage matrix, which is beneficial for cartilage repair and regeneration. On the other hand, COMP concentration is associated with the severity of RA, and its reduction suggests alleviation of joint inflammation and cartilage destruction, further supporting the efficacy of the self-assembled peptide scaffold loaded with BMSCs in improving the pathological state of the joint.

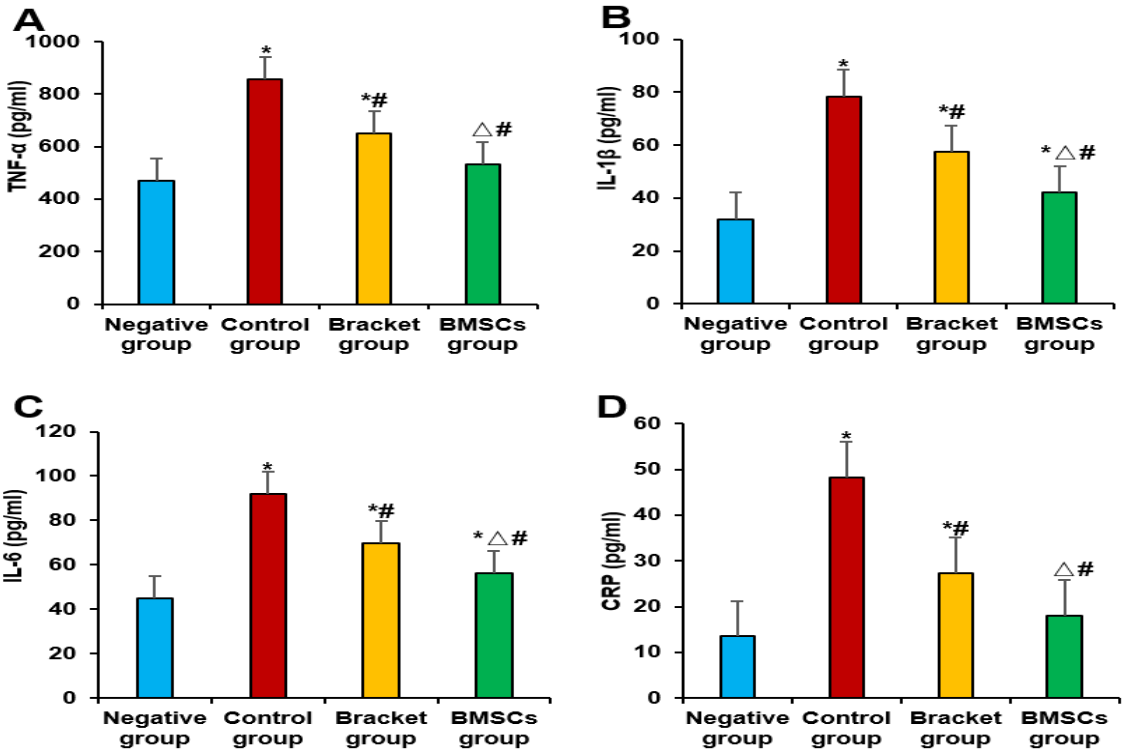

Fig 5. Comparison of inflammatory factor levels. A: TNF-α; B: IL-1 β; C: IL-6; D: CRP. *P≤0.05 vs. Negative group; #P≤0.05 vs. Control group; ΔP≤0.05 vs. Bracket group.

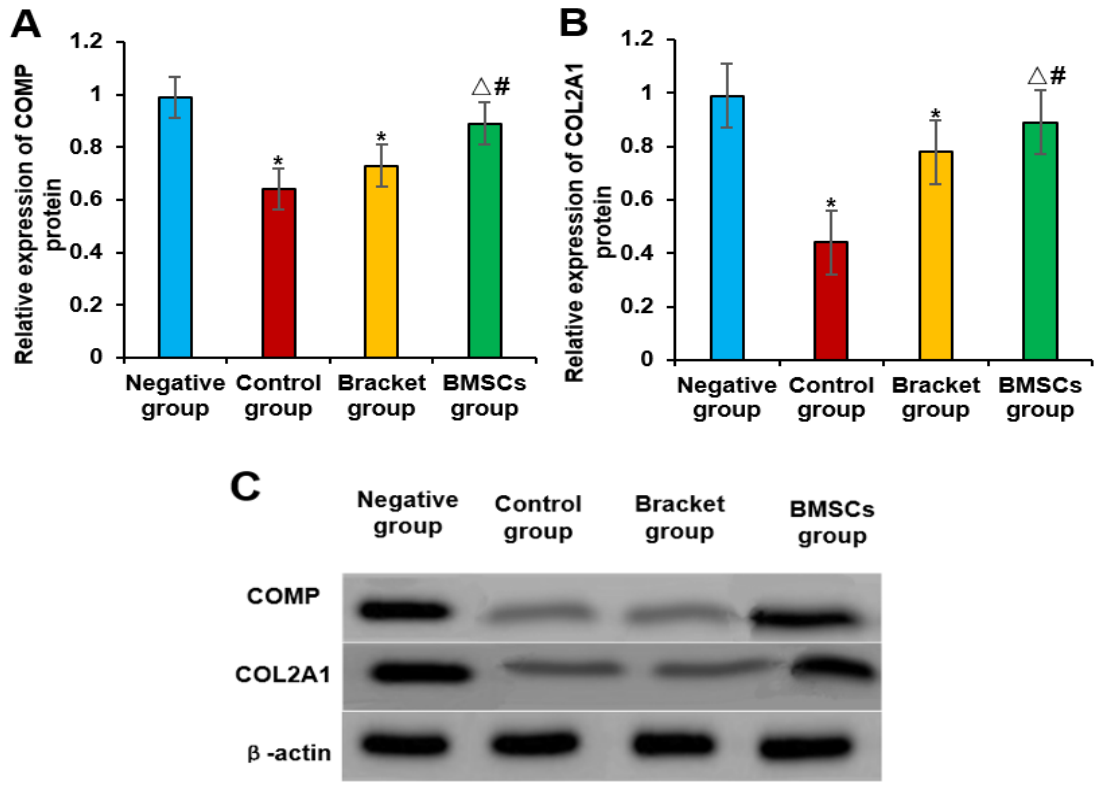

Fig 6.Relative expression levels of COMP and COL2A1 proteins and Western blotting results. A: relative expression level of COMP; B: relative expression level of COL2A1 protein; C: Western blotting results. *P≤0.05 vs. Negative group; #P≤0.05 vs. Control group; ΔP≤0.05 vs. Bracket group.

HE staining results of articular cartilage: The histological results from HE staining, as depicted in Fig. 7, reveal the condition of the knee joint cartilage integrity in Control group rabbits one month post-treatment. In Controlgroup, the integrity of the knee joint cartilage was severely compromised, with thinning of the cartilage and a reduction in superficial chondrocytes. The tidemark was also indistinct (Fig. 7A). The Bracket group and BMSCs group exhibited similar characteristics to Control group, including disrupted cartilage layers and decreased matrix staining (Fig. 7B and Fig. 7C). These histological findings align with the MRI statistical results. Following three months of treatment, in Control group rabbits, some vascular shadows were still observed in the histological staining images of the cartilage tissue (Fig. 7E), and the number of chondrocytes observed was similar to that at one month of treatment. In contrast, Bracketgroup and BMSCs group both showed varying degrees of improvement. The cartilage thickness increased, and there was diffuse proliferation of superficial chondrocytes. The number of chondrocytes observed in the field of view was markedly superior to that inControlgroup at the same time point. The cartilage matrix staining was well-preserved, and the tidemark was relatively clear without distinct vascular shadows (Fig. 7F and Fig. 7G). Furthermore, the therapeutic effect of BMSCs group was notably superior to Bracket group.Fig. 7D is a magnified view of the circled area in Fig. 7C, and Fig. 7H is a magnified view of the circled area in Fig. 7G. From the high magnification views, the proliferation of chondrocytes can be more clearly observed. The number of chondrocytes in BMSCs group was significantly increased, with a denser distribution, further confirming the promoting effect of the self-assembled peptide scaffold loaded with BMSCs on chondrocyte proliferation and cartilage repair.

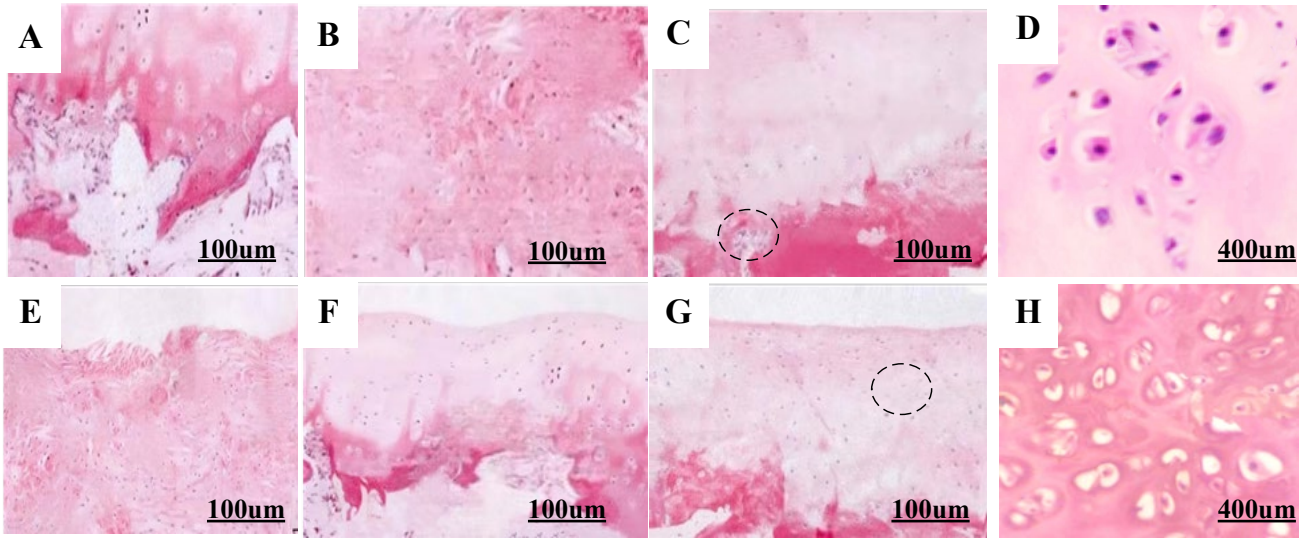

Fig7.HE staining of rabbit joint cartilage tissue at 1 month and 3 months post-treatment.(A, B, C, E, F, G: ×100; D, H: ×400). A:Control group at 1 month; B: Bracket group at 1 month; C: BMSCs group at 1 month; D: magnified view of the circled area in panel C; E: Controlgroup at 3 months; F: Bracket group at 3 months; G: BMSCs group at 3 months; H: magnified view of the circled area in panel G. The circles in panels C and G indicated the magnified areas.

Synovial pathology score: The Negative group showed no bone synovial pathology score. The histopathological scores of the synovial tissue in the four groups of rabbits are shown in Fig. 8. Nevertheless, noticeable differences emerged at the second and third months, with the disparities becoming particularly pronounced at the third month. These differences held statistical significance ($P \leq 0.05$).Within the first month of treatment, although no significant differences were observed in the evaluation indices among the four groups ($P > 0.05$), some indicators in Bracket group and BMSCs group showed a favorable trend. With the extension of the treatment period, by the second month, the peptide scaffold loaded in Bracket group and BMSCs cells began to take effect, gradually demonstrating repair effects on the synovium and cartilage. As a result, these two groups started to show better synovial pathology scores and cartilage Mankin scores compared to Control group, with statistically significant differences ($P \leq 0.05$). This suggests that treatment duration is a critical factor influencing the manifestation of therapeutic effects. Initially similar among the groups, Bracket group and BMSCs group gradually diverged with time, showing a trend of better treatment outcomes compared to Control group.

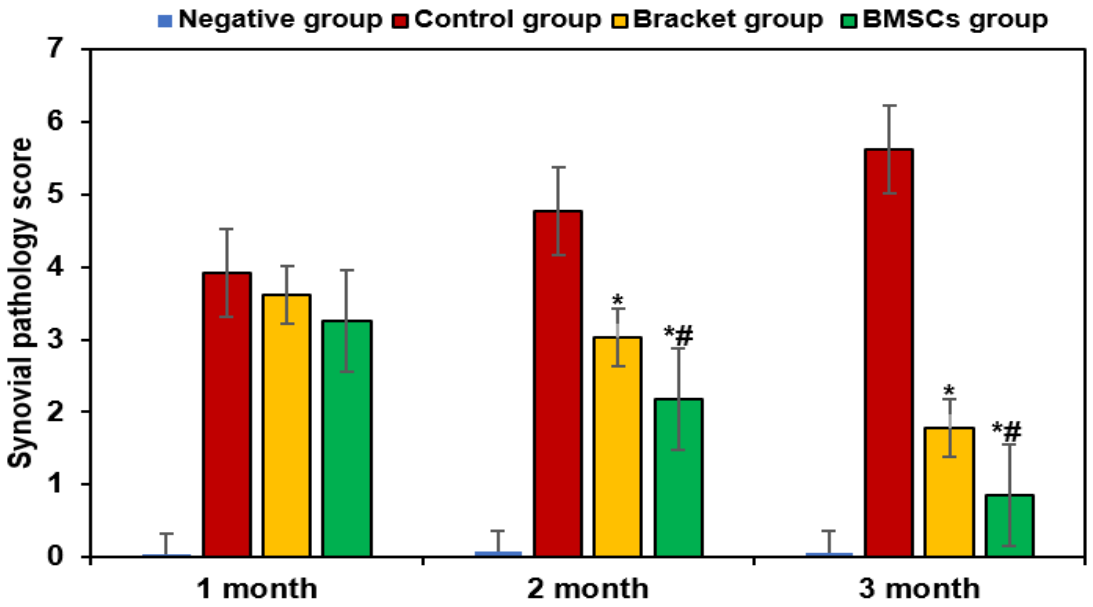

Fig 8. Comparison of pathological scores of cartilage synovium in each group of rabbits. *$P \leq 0.05$ vs. Control group; #$P \leq 0.05$ vs. Bracket group.

Cartilage Mankin score: The Negative group had no Mankin score. The Mankin scores of the other three groups are shown in Fig. 9. At each time point, BMSCs group had lower scores than Controlgroup and Bracket group($P \leq 0.05$). This indicates that from 1 to 3 months, the group loaded with BMSCs had relatively lower cartilage damage and better cartilage repair outcomes. The Bracket group had lower scores than Control group, suggesting that simply placing the peptide scaffold can also alleviate cartilage damage to some extent. From 1 to 3 months, Controlgroup scores showed little change, indicating that with only surgical joint exposure, the degree of cartilage damage remained relatively stable during this period. Both Bracket group and BMSCs group showed a downward trend in scores ($P \leq 0.05$), with BMSCs group showing a more significant reduction. This suggests that over time, both interventions can improve cartilage conditions, with BMSCs group showing a more pronounced improvement ($P \leq 0.05$).

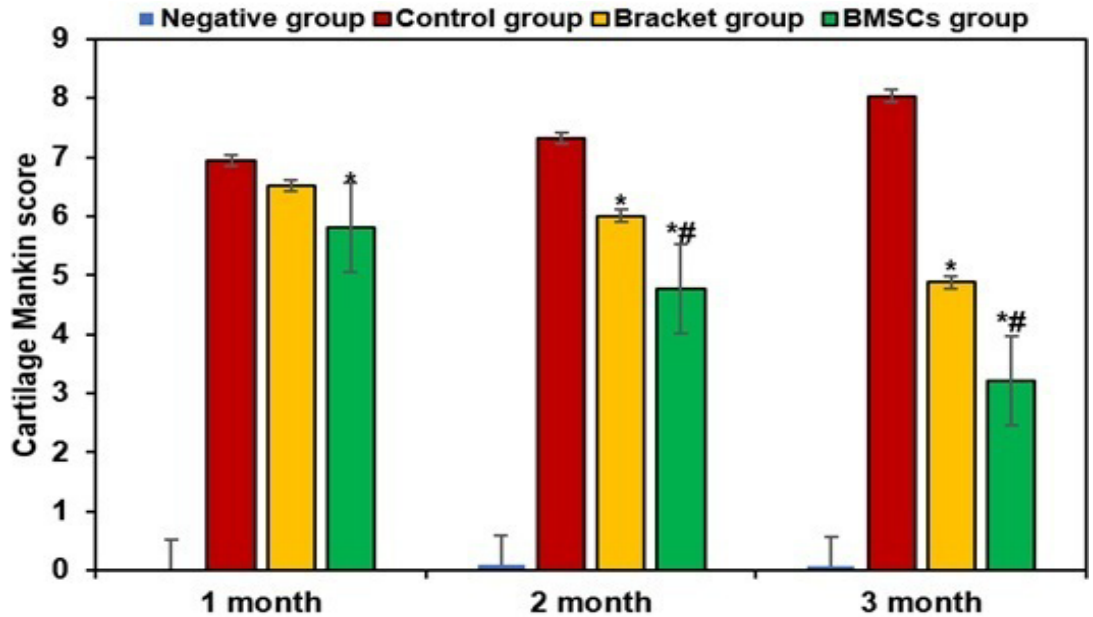

Fig 9. Comparison of Mankin scores of cartilages in each group of rabbits. *$P \leq 0.05$ vs. Control group; #$P \leq 0.05$ vs. Bracket group.

DISCUSSION

In this study, a composite scaffold material incorporating BMSCs was prepared using self-assembling peptides. Initially, the biocompatibility of this material was assessed, revealing a significant presence of nanofibers. Co-cultivation of BMSCs with the scaffold material resulted in enhanced cellular metabolic activity. The peptide scaffold exhibited abundant interconnected pores within its structure, facilitating excellent cell adhesion and integration with the scaffold, thereby supporting cell growth. BMSCs were found to adhere to the peptide scaffold without causing harm to rabbits, suggesting potential for promoting stem cell proliferation and differentiation for applications in tissue engineering and regenerative medicine. The multi-lineage differentiation potential of BMSCs and the active factors they secrete (such as VEGF and bFGF) play a key role in inhibiting inflammation and promoting cartilage regeneration. Notably, the combination of BMSCs with functionalized scaffold materials has shown broad application prospects in bone and cartilage repair. For example, in the field of bone regeneration, Zhou *et al.* developed a polydopamine-coated biomimetic bone scaffold (SCN/PDA-exo-functionalized), which significantly promoted BMSCs osteogenic differentiation and *in vivo* bone regeneration efficiency through the loading of exosomes (Zhou *et al*., 2023). Zhou *et al.* further demonstrated that the SF/CS/NHA composite scaffold combined with autologous concentrated growth factors synergistically enhanced BMSCs proliferation and osteogenic differentiation, significantly improving the repair efficiency of critical-sized bone defects (Zhou *et al*., 2022). Xiong *et al.* used miR-19b-3p-modified BMSCs combined with PLLA/POSS scaffolds to target the inhibition of the Smurf1 gene, significantly enhancing osteogenic activity and accelerating bone density recovery in bone defect areas (Xiong *et al*., 2020). Yu *et al.* achieved efficient cranial defect repair by co-transplanting endothelial progenitor cells and BMSCs using hyaluronic acid, chitosan, and polycaprolactone (HA/CS/PCL) composite scaffold, regulating the endogenous expression of BMP-2, VEGF, and PDGF (Yu *et al*., 2022). Subsequently, an animal model of RA was established. It was observed that the joints of the modeled rabbits exhibited more severe swelling accompanied by pain. Joint swelling is a primary symptom of RA, significantly impacting patients' quality of life (Heckert *et al*., 2022).

Furthermore, this study found that the severity of joint swelling and pain in a RA animal model was significantly improved following treatment with BMSCs and BMSCs loaded onto self-assembling peptide composite scaffolds. The therapeutic effect was notably more pronounced with the BMSC-loaded self-assembling peptide composite scaffolds. Treatment using BMSC-loaded self-assembling peptide scaffolds demonstrated a significant impact on joint swelling in the RA model. By reducing joint swelling, this treatment may contribute to alleviating pain, improving joint function, and slowing down joint structural damage.In this study, Bracket group (implanted with peptide scaffolds without BMSCs) also demonstrated improvements in cartilage thickness following treatment. This phenomenon suggests that the peptide scaffold alone may exert therapeutic effects independent of BMSCs. The peptide scaffold itself possesses excellent biocompatibility and a specific three-dimensional structure, with its abundant nanofibers and porous network potentially providing attachment sites for endogenous stem or progenitor cells within the joint, guiding their migration to the damaged cartilage region. The peptide scaffold may promote the proliferation and differentiation of endogenous cells by modulating the physical and chemical signals within the local microenvironment, thereby enhancing cartilage repair capacity. The study also indicates that self-assembled peptide scaffolds could create more favorable conditions for cartilage repair by influencing extracellular matrix components (*e.g.,* collagen fiber arrangement), while providing a stable support structure for chondrocytes, promoting matrix synthesis and secretion (Zhang *et al.,* 2022). Although the therapeutic effect of BMSCs group was more pronounced, the independent role of the scaffold should not be overlooked, providing theoretical support for the future development of scaffold materials that do not require the implantation of exogenous cells.

MRI imaging technology is used in the examination of RA and can clearly depict synovial hyperplasia, joint cartilage interface destruction, and the formation of intraosseous cysts (Ranganath *et al*., 2020; Bertham *et al*., 2022). In this study, MRI was employed to examine synovial hyperplasia and cartilage thickness changes in an RA animal model. It was found that immediately and at three months post-treatment with BMSC-loaded self-assembling peptide composite scaffolds, there was a significant reduction in synovial hypertrophy volume and an increase in cartilage thickness in the RA animal model. This indicates that BMSC-loaded self-assembling peptide scaffolds can effectively suppress excessive synovial proliferation, thereby reducing synovial volume. These findings are consistent with previous research and confirm the inhibitory effect of BMSC-loaded self-assembling peptide scaffolds on synovium (Hansson *et al*., 2020; Sunk *et al*., 2022). BMSCs possess multipotent differentiation capabilities and can differentiate into chondrocytes, producing cartilage matrix. This suggests that BMSC-loaded self-assembling peptide scaffolds may provide a better environment for cartilage repair and regeneration by inhibiting excessive synovial proliferation. Excessive synovial proliferation is a major pathological characteristic of RA that leads to joint

destruction and functional impairment (Yang *et al*., 2020). BMSC-loaded self-assembling peptide scaffolds can offer surfaces for cell adhesion and provide the necessary support for cell proliferation, thereby promoting chondrocyte proliferation and differentiation and increasing cartilage thickness (Knoll *et al*., 2020). Therefore, BMSC-loaded self-assembling peptide scaffolds, by simultaneously reducing synovial volume and increasing cartilage thickness, may have enhanced therapeutic effects. The Bracket group also exhibited significant improvement after treatment, which may be attributed to the good biocompatibility and bioactivity of the peptide scaffold itself. It provides a supportive and reparative environment for the joint tissues, promoting the repair of synovium and cartilage. However, compared to BMSCs group, the treatment effect in BMSCs group was more pronounced, indicating that the addition of BMSCs further enhanced the repair ability. This difference is of great significance for the clinical translation of this technology. This study showed that the MRI evaluation results demonstrated that the self-assembled peptide scaffolds loaded with bone marrow-derived mesenchymal stem cells (BMSCs) effectively reduced synovial volume and increased cartilage thickness. These structural improvements were closely associated with the recovery of joint function. The reduced synovial volume indicated alleviation of inflammation, which decreased the erosion of joint tissues, thereby relieving joint pain and swelling, and improving joint mobility. Meanwhile, the increased cartilage thickness enhanced the cushioning and protective functions of the joint, strengthening joint stability and promoting the recovery of joint function, ultimately improving the locomotor ability and quality of life of the experimental animals.

RA is an autoimmune disease characterized by erosive arthritis. When synovitis occurs, it leads to the generation of abundant inflammatory mediators, exacerbating local and systemic inflammatory reactions (Alivernini*et al*., 2020). TNF-α, IL-1β, IL-6, and CRP are commonly elevated inflammatory factors associated with inflammatory diseases, infections, and tissue damage (Yokota *et al*., 2021). This study further examined changes in the levels of inflammatory factors TNF-α, IL-1β, IL-6, and CRP in an RA animal model and found that their levels significantly decreased after treatment with BMSC-loaded self-assembling peptide composite scaffolds. This reduction in inflammatory factor levels suggests that mitigating inflammation may slow joint structural damage, protect cartilage and synovium, and promote healing. The BMSC scaffold exhibits the ability to suppress inflammatory factor levels, thereby facilitating the recovery from RA. RA is an autoimmune disease characterized by synovitis, which can ultimately lead to joint deformities. Joint cartilage is a target of progressive destruction in RA, with COL2A1 being an important component of joint cartilage (Samundeshwari *et al*., 2024). COMP is a non-collagenous glycoprotein produced by cartilage, synovium, tendons, and meniscus. COMP concentration is associated with the severity of RA, increasing as the disease progresses (Saghafi *et al*., 2017). This study found that after treating the RA animal model with BMSC-loaded self-assembling peptide composite scaffolds, the protein expression level of COL2A1 significantly increased while the expression level of COMP significantly decreased. The BMSC-loaded self-assembling peptide group positively influenced joint repair and regeneration in the RA animal model by modulating the expression of COL2A1 and COMP proteins, potentially improving joint function and structure. Furthermore, the study observed a significant reduction in synovial pathology scores and cartilage Mankin scores in the RA animal model following treatment with BMSC-loaded self-assembling peptide composite scaffolds. This suggests that the treatment may not have a significant effect initially but over time, it could positively impact the condition of the rabbits and lead to improvements in the Mankin score. BMSCs have the capability to differentiate into chondrocytes, contributing to cartilage tissue regeneration and repair (Pan *et al*., 2022; Li *et al*., 2021). Additionally, BMSCs can secrete various growth factors such as vascular endothelial growth factor (VEGF) and basic fibroblast growth factor (bFGF), which promote angiogenesis, alleviate inflammation, and stimulate tissue regeneration in the surrounding area (Wu *et al*., 2023). Therefore, it can be concluded that BMSC-loaded self-assembling peptide scaffolds play a therapeutic role in cartilage repair in rabbits.

Conclusion: Through the establishment of an RA model in rabbits, the loaded BMSCs with self-assembling peptide scaffolds have demonstrated potential therapeutic effects in the experimental model, particularly in addressing synovial hyperplasia and cartilage repair. These findings provide promising insights into the use of scaffolds in the treatment of RA.

Authors' Contributions: Rina Sha and Jizheng Li designed experiments; Rina Sha and Jizheng Li collected samples; Rina Sha and Jizheng Li performed experiments; Rina Sha and Jizheng Li analyzed data; Rina Sha and Jizheng Li wrote the manuscript. All authors agreed to publish this article.

Animal Rights Statement: The local Ethics Committee of Ordos Institute of Technology (Inner Mongolia Autonomous Region, China) had authorized the animal experiment project of this study.

Statement: All authors have no conflicts of interest.

REFERENCES

Alivernini, S., L. MacDonald, A. Elmesmari, S. Finlay, B. Tolusso, M.R. Gigante, L. Petricca, C. Di Mario, L. Bui, S. Perniola, M. Attar, M. Gessi, A.L. Fedele, S. Chilaka, D. Somma, S.N. Sansom, A. Filer, C. McSharry, N.L. Millar, K. Kirschner, A. Nerviani, M.J. Lewis, C. Pitzalis, A.R. Clark, G. Ferraccioli, I. Udalova, C.D. Buckley, E. Gremese, I.B. McInnes, T.D. Otto and M. Kurowska-Stolarska (2020). Distinct synovial tissue macrophage subsets regulate inflammation and remission in rheumatoid arthritis. Nat. Med.26(8):1295-1306. doi.org/10.1038/s41591-020-0939-8.

Arora, D. and P.G. Robey (2022). Recent updates on the biological basis of heterogeneity in bone marrow stromal cells/skeletal stem cells. Biomater. Transl.3(1):3-16. doi.org/10.12336/biomatertransl.2022.01.002.

Bertham, D.P., A.L. Tan, A. Booth, L. Paton, P. Emery, J. Biglands and M. Farrow (2022). Repeatability of quantitative MRI in patients with rheumatoid arthritis. Radiography (Lond).28(3): 831-837. doi.org/10.1016/j.radi.2022.01.004.

Chia, W., J. Liu, Y.G. Huang and C. Zhang (2020). A circular RNA derived from DAB1 promotes cell proliferation and osteogenic differentiation of BMSCs via RBPJ/DAB1 axis. Cell Death Dis.11(5): 372. doi.org/10.1038/s41419-020-2572-3.

Chen, G., Y. Zhuo, B. Tao, Q. Liu, W. Shang, Y. Li, Y. Wang, Y. Li, L. Zhang, Y. Fang, X. Zhang, Z. Fang and Y. Yu (2020). Moderate SMFs attenuate bone loss in mice by promoting directional osteogenic differentiation of BMSCs. Stem Cell Res. Ther.11(1):487. doi.org/10.1186/s13287-020-02004-y.

Deane, K.D. and V.M. Holers (2021). Rheumatoid arthritis pathogenesis, prediction, and prevention: an emerging paradigm shift. Arthritis Rheumatol,73(2),181-193. https://doi.org/10.1002/art.41417.

Heckert, S.L., S.A. Bergstra, X.M.E. Matthijssen, Y.P.M. Goekoop-Ruiterman, F. Fodili, S. Ten Wolde, C.F. Allaart and T.W.J. Huizinga (2022). Joint inflammation tends to recur in the same joints during the rheumatoid arthritis disease course. Ann. Rheum. Dis.81(2):169-174. doi.org/10.1136/annrheumdis-2021-220882.

Hansson, B., K. Markenroth Bloch, T. Owman, M. Nilsson, J. Lätt, J. Olsrud, and I.M. Björkman-Burtscher (2020). Subjectively reported effects experienced in an actively shielded 7T MRI: a large-scale study. J. Magn.Reson. Imaging.52(4):1265-1276. doi.org/10.1002/jmri.27139.

Hou, M., B. Tian, B. Bai, Z. Ci, Y. Liu, Y. Zhang, G. Zhou and Y. Cao (2021). Dominant role of *in situ* native cartilage niche for determining the cartilage type regenerated by BMSCs. Bioact. Mater.13: 149-160. doi.org/10.1016/j.bioactmat.2021.11.007.

Hansildaar, R., D. Vedder, M. Baniaamam, A.K. Tausche, M. Gerritsen, and M.T. Nurmohamed (2021). Cardiovascular risk in inflammatory arthritis: rheumatoid arthritis and gout. Lancet Rheumatol.3(1):e58-e70. doi.org/10.1016/S2665-9913(20)30221-6.

Jiao, D., A. Zheng, Y. Liu, X. Zhang, X. Wang, J. Wu, W. She, K. Lv, L. Cao and X. Jiang (2020). Bidirectional differentiation of BMSCs induced by a biomimetic procallus based on a gelatin-reduced graphene oxide reinforced hydrogel for rapid bone regeneration. Bioact. Mater.6(7):2011-2028. doi.org/10.1016/j.bioactmat.2020.12.003.

Knoll, F., K. Hammernik, C. Zhang, S. Moeller, T. Pock, D.K. Sodickson, and M. Akçakaya (2020). Deep-learning methods for parallel magnetic resonance imaging reconstruction: a survey of the current approaches, trends, and issues. IEEE Signal Process Mag. 37(1): 128-140. doi.org/10.1109/MSP.2019.2950640.

Kerschbaumer, A., A. Sepriano, J.S. Smolen, D. van der Heijde, M. Dougados, R. van Vollenhoven, I.B. McInnes, J.W.J. Bijlsma, G.R. Burmester, M. de Wit, L. Falzon and R. Landewé (2020). Efficacy of pharmacological treatment in rheumatoid arthritis: a systematic literature research informing the 2019 update of the EULAR recommendations for management of rheumatoid arthritis. Ann. Rheum. Dis.79(6):744-759. doi.org/10.1136/annrheumdis-2019-216656.

Kelly, C.N., C.E. Townsend, A.N. Jain, M.R. Naylor, C.R. Pye, J. Schwochert, and R.S. Lokey (2021). Geometrically diverse lariat peptide scaffolds reveal an untapped chemical space of high membrane permeability. J. Am. Chem. Soc.143(2): 705-714. doi.org/10.1021/jacs.0c06115.

Li, G.Q., Y.X. Fang, Y. Liu, F.R. Meng, X. Wu, C.W. Zhang, Y. Zhang, Y.Q. Liu and D. Liu (2021). MicroRNA-21 from bone marrow mesenchymal stem cell-derived extracellular vesicles targets TET1 to suppress KLF4 and alleviate rheumatoid arthritis. Ther. Adv. Chronic. Dis.12:20406223211007369. doi.org/10.1177/20406223211007369.

Liu, Y., L. Peng, L. Li, C. Huang, K. Shi, X. Meng, P. Wang, M. Wu, L. Li, H. Cao, K. Wu, Q. Zeng, H. Pan, W.W. Lu, L. Qin, C. Ruan and X. Wang

(2021). 3D-bioprinted BMSC-laden biomimetic multiphasic scaffolds for efficient repair of osteochondral defects in an osteoarthritic rat model. Biomaterials.279: 121216. doi.org/10.1016/j.biomaterials.2021.121216.

Liang, Q., Y. Tian, Z. Liu, D. Yu, H. Guo, and F. Sun (2023). Co-culture of bone marrow mesenchymal stem cells and fibroblast-like synoviocytes (RA-FLS) alleviates rheumatoid arthritis cell apoptosis by inhibiting inflammatory response. J. Biomater. Tissue Eng.13(2): 294-300. doi.org/10.1166/jbt.2023.3254.

Nagy, G., N.M.T. Roodenrijs, P.M. Welsing, M. Kedves, A. Hamar, M.C.van der Goes, A. Kent, M. Bakkers, E. Blaas, L. Senolt, Z. Szekanecz, E. Choy, M. Dougados, J.W. Jacobs, R. Geenen, H.W. Bijlsma, A. Zink, D. Aletaha, L. Schoneveld, P. van Riel, L.Gutermann, Y. Prior, E. Nikiphorou, G. Ferraccioli, G. Schett, K.L. Hyrich, U. Mueller-Ladner, M.H. Buch, I.B. McInnes, D. van der Heijde and J.M. van Laar.(2021). EULAR definition of difficult-to-treat rheumatoid arthritis. Ann. Rheum. Dis. 80(1): 31-35. doi.org/10.1136/annrheumdis-2020-217344.

Parmar, M., S. Grealish and C. Henchcliffe(2020). The future of stem cell therapies for Parkinson disease. Nat. Rev.Neurosci.21(2):103-115. doi.org/10.1038/s41583-019-0257-7.

Pan, S., L. Wang, B. Wu and H. Xing (2022). Effect and mechanism of siRNAs Targeting IL-1β/TNF-α combined with BMSCs transplantation in ameliorating rheumatoid arthritis in rats. Vet. Sci.9(10):531. doi.org/10.3390/vetsci9100531.

Radu, A.F. and S.G. Bungau (2021). Management of rheumatoid arthritis: an overview. Cells. 10(11): 2857. doi.org/10.3390/cells10112857.

Ranganath, V.K., H.B. Hammer, and F.M. McQueen (2020). Contemporary imaging of rheumatoid arthritis: Clinical role of ultrasound and MRI. Best Pract. Res. Clin.Rheumatol. 34(6):101593. doi.org/10.1016/j.berh.2020.101593.

Reda, R., A. Zanza, A. Mazzoni, A. Cicconetti, L. Testarelli and D. Di Nardo (2021). An update of the possible applications of Magnetic Resonance Imaging (MRI) in Dentistry: a literature review. J. Imaging.7(5):75. doi.org/10.3390/jimaging7050075.

Samundeshwari, E.L., S. Kattaru, S. Kodavala, C. Chandrasekhar and P.V. G.K. Sarma (2024). Prominent Expression of COL2A1, ACAN and IHH genes are observed in the differentiation of human hematopoietic stem cells into articular type of chondrocytes. Stem. Cell Rev. Rep. 20(5): 1370–1373. doi.org/10.1007/s12015-023-10665-4.

Sunk, I.G., L. Amoyo-Minar, B. Niederreiter, A. Soleiman, F. Kainberger, J.S. Smolen, D.Aletaha and K. Bobacz (2022). Dorso-ventral osteophytes of interphalangeal joints correlate with cartilage damage and synovial inflammation in hand osteoarthritis: a histological/radiographical study. Arthritis Res. Ther.24(1): 226. doi.org/10.1186/s13075-022-02911-w.

Saghafi, M., M. Khodashahi, N. Saadati, A. Azarian, Z. Rezaieyazdi, M. Salehi and M. Sahebari(2017). Relationship between cartilage oligomeric matrix protein (COMP) and rheumatoid arthritis severity. Electron Physician.9(12): 5940-5947. doi.org/10.19082/5940.

Tian, S., Y. Yan, X. Qi, X. Li and Z. Li (2019). Treatment of Type II collagen-induced rat rheumatoid arthritis model by Interleukin 10 (IL10)-Mesenchymal Stem Cells (BMSCs). Med. Sci. Monit. 25: 2923-2934. doi.org/10.12659/MSM.911184.

Wu, Y., M. Liu, H. Zhou, X. He, W. Shi, Q. Yuan, Y. Zuo, B. Li, Q. Hu and Y. Xie (2023). COX-2/PGE2/VEGF signaling promotes ERK-mediated BMSCs osteogenic differentiation under hypoxia by the paracrine action of ECs. Cytokine.161: 156058. doi.org/10.1016/j.cyto.2022.156058.

Xie, J., H. Shen, G. Yuan, K. Lin and J. Su (2021). The effects of alignment and diameter of electrospun fibers on the cellular behaviors and osteogenesis of BMSCs. Mater. Sci. Eng. C Mater. Biol Appl.120: 111787. doi.org/10.1016/j.msec.2020.111787.

Xiong, A., Y. He, L. Gao, G. Li, J. Weng, B. Kang, D. Wang and H. Zeng (2020). Smurf1-targeting miR-19b-3p-modified BMSCs combined PLLA composite scaffold to enhance osteogenic activity and treat critical-sized bone defects. Biomater. Sci. 8(21): 6069–6081. doi.org/10.1039/d0bm01251c

Yamanaka, S. (2020). Pluripotent Stem Cell-Based Cell Therapy-Promise and Challenges. Cell Stem. Cell.27(4): 523-531. doi.org/10.1016/j.stem.2020.09.014.

Yokota, K., K. Sato, T. Miyazaki, Y. Aizaki, S. Tanaka, M. Sekikawa, N. Kozu, Y. Kadono, H. Oda and T. Mimura (2021). Characterization and Function of Tumor Necrosis Factor and Interleukin-6-Induced Osteoclasts in Rheumatoid Arthritis. Arthritis Rheumatol. 73(7): 1145-1154. doi.org/10.1002/art.41666.

Yang, J., H. Shao, Y. Ma, L. Wan, Y. Zhang, J. Jiang, J. Du and G. Tang (2020). Quantitative ultrashort

echo time magnetization transfer (UTE-MT) for diagnosis of early cartilage degeneration: comparison with UTE-T2* and T2 mapping. Quant Imaging Med. Surg.10(1):171-183. doi.org/10.21037/qims.2019.12.04.

Yang, B., H. Yao, J. Yang, C. Chen, and J. Shi (2022). Construction of a two-dimensional artificial antioxidase for nanocatalytic rheumatoid arthritis treatment. Nat Commun.13(1):1988. doi.org/10.1038/s41467-022-29735-1.

Yu, H., L. Xia, X. Leng, Y. Chen, L. Zhang, X. Ni, J. Luo and W. Leng (2022). Improved repair of rabbit calvarial defects with hydroxyapatite/chitosan/polycaprolactone composite scaffold-engrafted EPCs and BMSCs. Front. Bioeng. Biotechnol. 10: 928041. doi.org/10.3389/fbioe.2022.928041.

Zhou, Y., G. Deng, H. She, F. Bai, B. Xiang, J. Zhou and S. Zhang (2023). Polydopamine-coated biomimetic bone scaffolds loaded with exosomes promote osteogenic differentiation of BMSC and bone regeneration. Regen. Ther. 23:25-36. doi: 10.1016/j.reth.2023.03.005. PMID: 37063095; PMCID: PMC10091039.

Zhou, Y., X. Liu, H. She, R. Wang, F. Bai and B. Xiang (2022). A silk fibroin/chitosan/nanohydroxyapatite biomimetic bone scaffold combined with autologous concentrated growth factor promotes the proliferation and osteogenic differentiation of BMSCs and repair of critical bone defects. Regen. Ther. 21:307-321. doi: 10.1016/j.reth.2022.08.006. PMID: 36110973; PMCID: PMC9459434.